Combined photoelectron spectroscopy and ab initio study of the hypermetallic Al3C molecule

ARTICLE *in* THE JOURNAL OF CHEMICAL PHYSICS · MAY 1999

Impact Factor: 2.95 · DOI: 10.1063/1.478816

Combined photoelectron spectroscopy and *ab initio* study of the hypermetallic Al_3C molecule

Alexander I. Boldyrev and Jack Simons
Department of Chemistry, The University of Utah, Salt Lake City, Utah 84112

Xi Li, Wenwu Chen, and Lai-Sheng Wang
Department of Physics, Washington State University, Richland, Washington 99352 and W. R. Wiley Environmental Molecular Sciences Laboratory, Pacific Northwest National Laboratory, MS K8-88, P.O. Box 999, Richland, Washington 99352

(Received 28 December 1998; accepted 12 February 1999)

The chemical structure and bonding of the hypermetallic Al_3C and Al_3C^- species have been studied by photoelectron spectroscopy and *ab initio* calculations. Al_3C^- is found to have a planar triangular (D_{3h}, $^1A_1'$) structure (when averaged over zero-point vibrational modes) and Al_3C is found to have a triangular distorted planar structure (C_{2v}, $^2B_2$) with one elongated Al–C bond. Four peaks in the photoelectron spectra of Al_3C^- were identified at 2.56, 2.69, 3.23, and 4.08 eV. Assignment of the observed features was made on the basis of the *ab initio* calculations. The experimental adiabatic electron affinity of Al_3C was measured to be 2.56 ± 0.06 eV, compared to 2.47 eV calculated at the CCSD(T)+OVGF/6-311+G(2df) level of theory. The excellent agreement between the calculated and experimental electron affinity, vibrational frequencies, and excitation energies allowed us to completely elucidate the geometrical and electronic structure of the Al_3C molecule and its anion. [S0021-9606(99)01018-1]

INTRODUCTION

A number of hyperaluminum molecules, Al_3O (Refs. 1–5), Al_4O (Refs. 2, 6), Al_nN ($n=3,4$) (Refs. 6, 7), and Al_nS ($n=3-9$) (Ref. 8), with the number of ligands larger than what may be expected based on the octet rule, have been studied in the literature. In a sense, hyperaluminum species can be regarded as aluminum clusters bound ionically to a centrally located ''impurity'' heteroatom. The substantial stability of these molecules is due to the high degree of ionic character in the bonding between the central atom and ligands as well as bonding interactions among the ligand aluminum atoms.[2] This contrasts with ordinary molecules in which the only bonding interactions are between the central atom and its attached atoms or ''ligands,'' e.g., CH_4, CF_4, NH_3, NF_3, F_2O, and H_2O, etc., where the ligand–ligand interactions are repulsive. Hence, the usual valence theory, which does not include ligand–ligand bonding interactions is *not* able to predict the structure and stability of the hypermetallic molecules.

In this article we report a combined photoelectron spectroscopy (PES) and *ab initio* study of the Al_3C^- and Al_3C species, which have not been investigated previously. PES of size-selected anions combined with a laser vaporization cluster source has been proven to be a powerful experimental technique to study the electronic structure of a wide range of novel molecular and cluster species.[7,9–21] The PES spectra of Al_3C^- revealed four detachment channels, corresponding to the ground and first three excited states of Al_3C. *Ab initio* calculations were performed for both the anion and neutral. The calculated electron affinity, vibrational frequencies, and excitation energies are in good agreement with the experiment, thus allowing us to completely characterize the geometrical and electronic structure of the Al_3C molecule and its Al_3C^- anion.

EXPERIMENT

The experiments were performed with a magnetic-bottle time-of-flight (TOF) PES apparatus. Details of the experiment have been described in our previous publications.[22,23] Briefly, Al_3C^- was produced by a laser vaporization cluster source. An intense laser pulse (532 nm) from a Q-switched Nd:YAG laser was focused onto a pure Al target. Sufficient Al_3C^- mass signals were produced due to carbon impurity in the Al target. A mixed Al/C target was also used, but it favored clusters with high C content ($Al_3C_x^-$, $x>1$) and Al_3C^- was not produced more abundantly. The clusters formed from the laser vaporization source were entrained in a He carrier gas and underwent a supersonic expansion. The anion species in the beam were extracted perpendicularly into a TOF mass spectrometer. Al_3C^- was selected and decelerated before photodetachment by a laser beam. For the current experiment, three detachment photon energies were used, 355 (3.496 eV), 266 (4.661 eV), and 193 nm (6.424 eV). The resolution was better than 30 meV for 1 eV electrons at 355 and 266 nm and it was slightly poorer at 193 nm.

COMPUTATIONAL METHODS

We optimized the geometries of Al_3C and Al_3C^- employing analytical gradients with polarized split-valence basis sets (6-311+G*)[24–26] at the hybrid method which includes a mixture of Hartree–Fock exchange with density functional exchange-correlation method (B3LYP),[27–29] at the

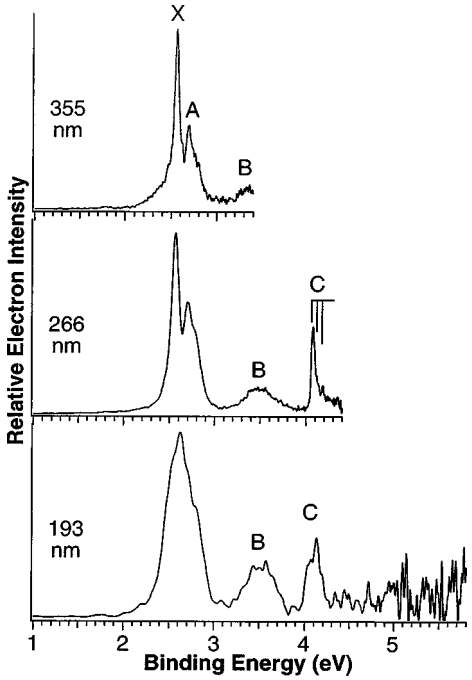

FIG. 1. Photoelectron spectra of Al_3C^- at 355, 266, and 193 nm. The four observed detachment channels are labeled (X, A, B, and C).

MP2(full) level of theory (meaning all electrons were included in the correlation calculations).[30] For the most stable structures, we employed the CCSD(T) method[31–33] in all our geometry and frequency calculations using the same basis sets. Finally, the energies of the lowest structures were refined using the CCSD(T) level of theory and 6-311 +G(2df) basis sets. The core electrons were kept frozen in treating the electron correlation at the CCSD(T) level of theory.

Vertical electron detachment energies of the two lowest singlet structures of Al_3C^- were calculated using outer valence Green function (OVGF) method[34–38] incorporated in GAUSSIAN 94. The 6-311+G(2df) basis sets were used in the OVGF calculations. All calculations were performed using the GAUSSIAN 94 program.[39]

EXPERIMENTAL RESULTS

The PES spectra of Al_3C^- are shown in Fig. 1 at three photon energies. The 355 nm spectrum gave three features, a sharp peak at 2.56 eV (X), a second band (A) at 2.69 eV with discernible vibrational progression (~610 cm^{-1} spacing), and a weak feature (B) at about 3.3 eV. The latter was observed more clearly in the 266 nm spectrum and was shown to be rather broad. The 266 nm spectrum also revealed an additional feature (C) with what appears to be a short vibrational progression of approximately 400 cm^{-1} spacing (see Table I). This vibrational progression was rather unusual, in that the $v=2$ appeared to be quite strong. The 193 nm spectrum had very low count rates and poor statistics (especially at high binding energies) and did not reveal any new features except that the relative intensity of the B feature was enhanced. In all three spectra, a substantial tail on the low binding energy side was present. The magnitude of this tail could be changed by varying experimental conditions, but could not be eliminated. It most likely consisted of contributions from hot band transitions. The observed binding energies and vibrational frequencies for all the observed features are summarized in Table I.

The PES features represent transitions from the ground state of the anion to the ground and low-lying excited states of the neutral. The binding energy of the transition to the ground state defines the adiabatic electron affinity of the neutral, which is measured to be 2.56 eV for Al_3C.

THEORETICAL RESULTS

At the B3LYP/6-311+G* level of theory, the global minimum of Al_3C^- was found to have a singlet $D_{3h}(^1A_1')$ structure (Table II) with a $1a_1'^2 1e'^4 2a_1'^2 1a_2''^2 2e'^4 3e'^0$ valence electron configuration. However, at both MP2(full)/6-311+G* and CCSD(T)/6-311+G* levels of theory, the $D_{3h}(^1A_1')$ structure was a saddle point. Following its imaginary frequency distortion, geometry optimization led to a $C_{3v}(^1A_1,\ 1a_1^2 1e^4 2a_1^2 3a_1^2 2e^4 3e^0)$ pyramidal structure (Table II), which was a global minimum for the Al_3C^- stoichiometry. The inversion barrier connecting pairs of such pyramidal structures is very small, only 35 cm^{-1} at the CCSD(T)/6-311+G* level of theory. Therefore, when zero-point energy corrections were added to both the C_{3v} and D_{3h} structures of Al_3C^-, the inversion barrier disappeared and the vibrationally averaged structure of Al_3C^- changed to D_{3h}. Therefore, we will use the $D_{3h}(^1A_1')$ structure in our further analysis of the Al_3C^- anion.

In Table I, we present our results of the OVGF/6-311+G(2df) calculations of all low-lying vertical one-electron detachment processes from the ground state Al_3C^-

TABLE I. Calculated and experimental electron detachment processes of Al_3C^-.

State	Experiment VDE (eV)	Experiment ADE (eV)	Experiment vib. freq.	C_{3v} state	Theory, VDE[a], (eV)	D_{3h} state	Theory, VDE[a] (eV)	State	Theory, AEDE
X	2.56(2)	2.56(2)		^2E	2.81 (0.875)[b]	$^2E'$	2.81 (0.874)[b]	$^2B_2$	2.47 eV[c]
A	2.69(4)	2.69(4)	610(60) cm^{-1}						
B	3.48(6)	3.23(6)		$^2A_1$	3.58 (0.862)[b]	$^2A_2''$	3.58 (0.861)[b]	$^2A_2''$	3.21 eV[d]
C	4.08(3)	4.08(3)	440(50) cm^{-1}	$^2A_1$	4.43 (0.860)[b]	$^2A_1'$	4.38 (0.866)[b]	$^2A_1'$	4.11 eV[d]
				^2E	7.09 (0.805)[b]	$^2E'$	7.09 (0.805)[b]		

[a]At the OVGF/6-311+G(2df) level of theory using CCSD(T)/6-311+G* geometry.
[b]Polestrength is given in parentheses.
[c]Calculated using the spin-pure CCSD(T) plus OVGF method (see text).
[d]At the CCSD(T)/6-311+G(2df) level of theory using CCSD(T)/6-311+G* geometry.

TABLE II. Calculated molecular properties of Al_3C^- structures.

$Al_3C^-(D_{3h}, {}^1A_1')$	$Al_3C^-(C_{3v}, {}^1A_1)$
B3LYP/6-311+G*[a]	
$E_{tot}=-765.473\,98$ au	
R(C–Al)=1.897 Å	
∠AlCAl=120.0°	
$\nu_1(a_1')=408\ cm^{-1}$	
$\nu_2(a_2'')=173\ cm^{-1}$	
$\nu_3(e')=842\ cm^{-1}$	
$\nu_4(e')=131\ cm^{-1}$	
MP2(full)/6-311+G*	MP2(full)/6-311+G*
$E=-764.315\,56$ au	$E=-764.315\,82$ au
$\Delta E=0.007$ eV	$\Delta E=0.0$ eV
R(C–Al)=1.895 Å	R(C–Al)=1.896 Å
∠AlCAl=120.0°	∠AlCAl=118.9°
$\nu_1(a_1')=414\ cm^{-1}$	$\nu_1(a_1)=428\ cm^{-1}$
$\nu_2(a_2'')=149i\ cm^{-1}$	$\nu_2(a_1)=121\ cm^{-1}$
$\nu_3(e')=861\ cm^{-1}$	$\nu_3(e)=855\ cm^{-1}$
$\nu_4(e')=113\ cm^{-1}$	$\nu_4(e)=121\ cm^{-1}$
CCSD(T)/6-311+G*	CCSD(T)/6-311+G*
$E=-763.96921$ au	$E=-763.969\,37$ au
$\Delta E=0.004$ eV	$\Delta E=0.0$ eV
R(C–Al)=1.897 Å	R(C–Al)=1.897 Å
∠AlCAl=120.0°	∠AlCAl=119.2°
$\nu_1(a_1')=414\ cm^{-1}$	$\nu_1(a_1)=425\ cm^{-1}$
$\nu_2(a_2'')=131i\ cm^{-1}$	$\nu_2(a_1)=144\ cm^{-1}$
$\nu_3(e')=858\ cm^{-1}$	$\nu_3(e)=855\ cm^{-1}$
$\nu_4(e')=114\ cm^{-1}$	$\nu_4(e)=119\ cm^{-1}$
CCSD/6-311+G(2df)[a]	CCSD(T)/6-311+G(2df)[a]
$E=-764.025884$ au	$E=-764.025\,58$ au
$\Delta E=0.008$ eV	$\Delta E=0.0$ eV

[a]At the CCSD(T)/6-311+G* optimal geometry.

anion. We stress that OVGF results are free from spin contaminations and symmetry breaking problems. One can see that the lowest vertical detachment energy (VDE) at this level of theory (2.81 eV) corresponds to removal of an electron from the $2e'$ HOMO, and thus produces a pair of neutral-molecule states. The second VDE (3.58 eV) corresponds to electron detachment from the $1a_2''$ MO and is well separated from the first transition. The third VDE at 4.38 eV corresponds to electron detachment from the $2a_1'$ MO, and the fourth VDE at 7.75 eV corresponds to electron detachment from the $1e'$ MO. In all cases, polestrengths are around 0.9; therefore the OVGF method is expected to be valid and all these electron detachments can be considered as primarily one-electron processes. This qualitative picture of the vertical electron detachment energies is in excellent agreement with the experimentally observed spectra as illustrated in Fig. 1.

INTERPRETATION OF THE PES SPECTRA

Peak X

Removal of an electron from the HOMO of Al_3C^- leads to a $^2E\,(1a_1{}^21e^42a_1{}^23a_1{}^22e^3)$ ground state for Al_3C neutral, which is expected to undergo Jahn–Teller distortion[40–42] toward C_{2v} symmetry. We optimized the structures of the two states that derive from this ^2E pair, C_{2v} ($^2B_2$, $1a_1{}^21b_2{}^22a_1{}^23a_1{}^21b_1{}^24a_1{}^22b_2{}^1$) and C_{2v} ($^2A_1$, $1a_1{}^21b_2{}^22a_1{}^23a_1{}^21b_1{}^24a_1{}^12b_2^2$), at the B3LYP/6-311+G* level of theory (Table III). The C_{2v} ($^2B_2$) state was found to produce a minimum (with all positive vibrational frequencies) and the C_{2v} ($^2A_1$) state generated a saddle point (with one imaginary frequency) on the intramolecular rearrangement of the Al_3C molecule from one global minimum into another equivalent structure. However, when these two structures were then examined at the MP2(full)/6-311+G* and CCSD(T)/6-311+G* levels of theory, the C_{2v} ($^2A_1$) saddle point structure was found to be lower in energy than the C_{2v} ($^2B_2$) minimum-energy structure. Unfortunately, the spin contamination was rather high for both of the above structures, so the MP2(full)/6-311+G* and CCSD(T)/6-311+G* results may not be reliable. For this reason, we had to examine other ways for determining the energies of the C_{2v} ($^2A_1$) and C_{2v} ($^2B_2$) states.

To circumvent the spin-contamination problem, we used an alternative approach in which the total energy of each state of the neutral Al_3C molecule was calculated by substracting from the total energy of the anion Al_3C^-, computed at the CCSD(T)/6-311+G(2df) level of theory, the corresponding vertical electron detachment energy of the anion computed at the OVGF/6-311+G(2df) level of theory (for which there is no spin-contamination). We started from the geometries predicted to be minimum-energy C_{2v} ($^2B_2$) and saddle-point C_{2v} ($^2A_1$) geometries by the CCSD(T)/6-311+G* level of theory, and then examined small geometric distortions (with $\Delta R=0.05$ Å and $\Delta\Phi=2°$) at which we computed the neutral states' energies in the above CCSD(T)+OVGF manner. The resulting optimal geometries of both neutral states, C_{2v} ($^2B_2$) and C_{2v}($^2A_1$), were found to be practically the same as had been obtained in the spin-contaminated calculations, and, again the $^2B_2$ state was found to be a minimum and the $^2A_1$ state to be a saddle point. However, in these spin-pure calculations, the C_{2v} ($^2B_2$) structure was found to be lower in energy than the C_{2v} ($^2A_1$) structure by 0.3 eV. Therefore, we conclude that the C_{2v} ($^2B_2$) structure is the global minimum and the C_{2v} ($^2A_1$) structure is a saddle point, and that the lowest adiabatic detachment energy (ADE), assuming a transition to the C_{2v} ($^2B_2$) state, is 2.47 eV (see Table I), which is in excellent agreement with the experimental value of 2.56 $\pm$0.06 eV.

Peak A

Peaks X, A, B, and C occur, respectively, near 2.56, 2.69, 3.48, and 4.08 eV. The lowest computed vertical detachment energies are 2.81, 3.58, 4.38, and 7.75 eV, with the first and last of these corresponding to producing degenerate E states of the neutral. As will be shown below in the following two subsections, the OVGF detachment energies at 3.58 and 4.38 ev account nicely for peaks B and C in the experiments, and the vertical detachment energy at 7.75 eV seems to be out of the range of any of the experimental features. Finally, as discussed above, one component of the degenerate ^2E state having a *vertical* detachment energy of 2.81 eV (specifically, the $^2B_2$ component lying 0.3 eV below

TABLE III. Calculated molecular properties of Al_3C structures.

$Al_3C(C_{2v}, {}^2B_2)$	$Al_3C(C_{2v}, {}^2A_1)$	$Al_3C(D_{3h}, {}^2A_2'')$	$Al_3C(D_{3h}, {}^2A_1')$
B3LYP/6-311+G*	B3LYP/6-311+G*	MP2(full)/6-311+G*	MP2(full)/6-311+G*
$E_{tot}=-765.385\,84$ au	$E=-765.385\,65$ au	$E=-764\,198\,86$ au	$E=-764.163\,06$ au
$\langle S^2\rangle=0.764$	$\langle S^2\rangle=0.766$	$\langle S^2\rangle=0.758$	$\langle S^2\rangle=0.783$
AEDE=2.40 eV	AEDE=2.40 eV	AEDE-3.18 eV	AEDE=4.15 eV
$R(C-Al_1)=1.975$ Å	$R(C-Al_1)=1.845$ Å	$R(C-Al)=1.996$ Å	$R(C-Al)=1.875$ Å
$R(C-Al_{2,3})=1.872$ Å	$R(C-Al_{2,3})=1.936$ Å	$\angle AlCAl=120.0°$	$\angle AlCAl=120.0°$
$\angle Al_1CAl_{2,3}=122.7°$	$\angle Al_1CAl_{2,3}=118.2°$	$\nu_1(a_1')=363\ cm^{-1}$	$\nu_1(a_1')=441\ cm^{-1}$
$\nu_1(a_1)=787\ cm^{-1}$	$\nu_1(a_1)=853\ cm^{-1}$	$\nu_2(a_2'')=(901)\ cm^{-1}$[a]	$\nu_2(a_2'')=263\ cm^{-1}$
$\nu_2(a_1)=384\ cm^{-1}$	$\nu_2(a_1)=385\ cm^{-1}$	$\nu_3(e')=702\ cm^{-1}$	$\nu_3(e')=896\ cm^{-1}$
$\nu_3(a_1)=111\ cm^{-1}$	$\nu_3(a_1)=123\ cm^{-1}$	$\nu_4(e')=133\ cm^{-1}$	$\nu_4(e')=174\ cm^{-1}$
$\nu_4(b_1)=163\ cm^{-1}$	$\nu_4(b_1)=166\ cm^{-1}$		
$\nu_5(b_2)=498\ cm^{-1}$	$\nu_5(b_2)=286\ cm^{-1}$		
$\nu_6(b_2)=101\ cm^{-1}$	$\nu_6(b_2)=146i\ cm^{-1}$		
CCSD(T)/6-311+G*	CCSD(T)/6-311+G*	CCSD(T)/6-311+G*	CCSD(T)/6-311+G*
$E=-763.882\,70$ au	$E=-763.883\,07$ au	$E=-763.861\,99$ au	$E=-763.824\,27$ au
$\langle S^2\rangle=0.998$	$\langle S^2\rangle=1.076$	$\langle S^2\rangle=0.758$	$\langle S^2\rangle=0.783$
AEDE=2.36 eV	AEDE=2.35 eV	AEDE=2.92 eV	AEDE=3.95 eV
$R(C-Al_1)=1.976$ Å	$R(C-Al_1)=1.839$ Å	$R(C-Al)=1.998$ Å	$R(C-Al)=1.887$ Å
$R(C-Al_{2,3})=1.876$ Å	$R(C-Al_{2,3})=1.946$ Å	$\angle AlCAl=120.0°$	$\angle AlCAl=120.0°$
$\angle Al_1CAl_{2,3}=124.9°$	$\angle Al_1CAl_{2,3}=115.7°$		
CCSD(T)/6-311+G(2df)[b]	CCSD(T)/6-311+G(2df)[b]	CCSD(T)/6-311+G(2df)[b]	CCSD(T)/6-311+G(2df)[b]
$E=-763.93149$ au	$E=-763.93205$ au	$E=-763.907695$ au	$E=-763.874\,69$ au
AEDE=2.56 eV	AEDE=2.55 eV	AEDE=3.21 eV	AEDE=4.11 eV

[a]There is a symmetry broken problem for the vibration at this level of theory.
[b]At the CCSD(T)/6-311+G* optimal geometry.

^2E and thus at an adiabatic detachment energy of 2.5 eV) accounts remarkably well for the X peak in the spectrum. Therefore the peak A observed near 2.7 eV most likely relates to the second state (i.e., the $^2A_1$ state) deriving from the ^2E pair lying at 2.81 eV. The C_{2v} geometrical *structure* for this $^2A_1$ state discussed above as a saddle point cannot be associated with peak A because this structure is not geometrically stable. Peak A must be associated with a transition to some other geometrical structure on this $^2A_1$ energy surface.

Another possibility is that peak A could be vibrational structure in the peak X transition. However, according to our calculations, no vibrational frequency is large enough to account for the $>1000\ cm^{-1}$ energy separation between peaks X and A. Therefore, we tentatively assign peak A to a transition into the second state (i.e., the $^2A_1$ state) of the Jahn–Teller pair of states derived from the ^2E pair.

Peak B

The third vertical electron detachment energy (peak B) was found to be 3.48 ± 0.06 eV (Table I), which agrees well with the calculated value 3.58 eV at the OVGF/6-311+G(2df) level of theory, corresponding to vertical detachment from the $1a_2''$-MO(HOMO-1) resulting in a D_{3h}, $^2A_2''$ $(1a_1'^{\,2}1e'^{\,4}2a_1'^{\,2}1a_2''^{\,1}2e'^{\,4}3e'^{\,0})$ state. This is a nonbonding MO composed primarily of the $2p_\pi$-AO of the carbon atom (Fig. 2). After geometry optimization of the D_{3h} $^2A_2''$ structure, we found it to be a local minimum with a substantial elongation of the Al–C bonds by 0.1 Å at the CCSD(T)/6-311+G* level of theory (Table III), consistent with the broad nature of this transition. The MP2(full)/6-311+G* and CCSD(T)/6-311+G* calculations of the D_{3h} $^2A_2''$ state are almost free from spin-contaminations, but the ν_2 frequency experienced a symmetry breaking problem at the MP2(full)/6-311+G* level of theory. The adiabatic electron detachment energy was calculated to be 3.21 eV at the CCSD(T)/6-311+G(2df) level of theory, again in excellent agreement with the experimental value of 3.23 ± 0.09 eV (Table I).

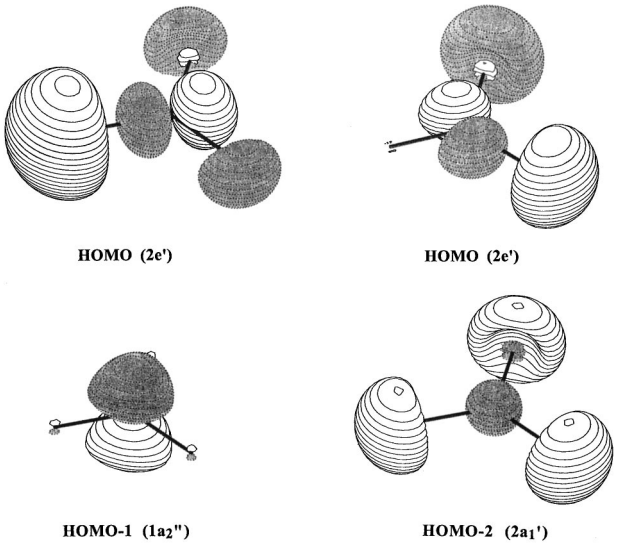

FIG. 2. Molecular orbital pictures (Ref. 43) of the D_{3h} Al_3C^-, showing the degenerate HOMO $(2e')$, HOMO−1 $(1a_2'')$, and HOMO−2 $(2a_1')$, from which electron detachment was observed in the current experiment.

Peak C

The fourth peak C can be assigned to detachment of an electron from the $2a_1'$-MO resulting in the D_{3h}, $^2A_1'$ ($1a_1'^2 1e'^4 2a_1'^1 1a_2''^2 2e'^4 3e'^0$) state. This (Fig. 2) is an antibonding MO with respect to the central atom–ligand interactions and is composed primarily of the $2s$-AO of carbon and $3s$-AO of aluminum atoms with some hybridization with the $3p$-AO. The VDE was calculated to be 4.43 eV at the OVGF level of theory. The D_{3h} $^2A_1'$ state was found to be a local minimum with the C–Al bond being essentially the same as in the Al_3C^- anion (Table III). The MP2(full)/6-311+G* and CCSD(T)/6-311+G* calculations are again almost free from spin-contamination. The ADE was calculated to be 4.11 eV at the CCSD(T)/6-311+G(2df) level of theory, in excellent agreement with the experimental value 4.08 ± 0.03 eV (Table I). The structure of the D_{3h} $^2A_1'$ state is nearly identical to that of the anion, consistent with the sharp detachment feature observed. Based on the fact that there is little geometry change between this state and the anion, no vibrational excitation should be observed in the photodetachment transition. However, a short vibrational progression was observed in the C band and the frequency (ca. 400 cm^{-1}) was in excellent agreement with that calculated for the totally symmetric mode (ν_1). However, we observed that the intensity of the $v=2$ feature in the C band was unusually high and noted that the calculated frequency of the $\nu_3(e')$ mode (Table III) is nearly identical in energy to two quanta of the ν_1 mode. Therefore, the unusual intensity pattern could alternatively be due to excitation of $\nu_3(e')$ mode. At this time, we cannot resolve this issue.

DISCUSSION

Overall, we obtained excellent agreement between experimental and *ab initio* results, allowing us to conclude that the structure of both Al_3C^- and Al_3C have been established with reasonable certainty. Al_3C^- is found to have a planar triangular (D_{3h}, $^1A_1'$) structure (when averaged over zero-point vibrational modes) and Al_3C is found to have a triangular distorted planar structure (C_{2v}, $^2B_2$) with one elongated Al–C bond.

The electron affinity of the Al_3C molecule (2.56 ± 0.06 eV) found in this work is substantially higher than the electron affinity of the pure Al_3 cluster (1.90 ± 0.03 eV),[4,20] of Al_3O (1.14 ± 0.06 eV),[4] or of Al_3N (0.96 ± 0.08 eV).[7] As one can see from these results, an impurity atom may affect the electron affinity of the Al_3 cluster in both directions: the electron affinity can be increased by inserting a carbon atom inside the Al_3 cluster or decreased when an oxygen or nitrogen atom is inserted inside the Al_3 cluster. In all three Al_3X (X=C, N, O) molecules, the structures with X inside the cluster was found to be the global minima. Therefore, knowing the influence of impurity atoms on clusters, their electronic properties can be modified in a desirable direction. Further studies will be needed to completely understand the unique chemical bonding properties of the hypermetallic cluster species and to design a theory of the influence of impurity atoms on the physical and chemical properties of these clusters.

ACKNOWLEDGMENTS

The theoretical work done in Utah is supported by the National Science Foundation (CHE-9618904). The authors acknowledge the Center for High Performance Computations at the University of Utah for computer time. The experimental work done at Washington is supported by the National Science Foundation (DMR-9622733). We thank Dr. H. Wu for experimental assistance. The experiment was performed at the W. R. Wiley Environmental Molecular Sciences Laboratory, a national scientific user facility sponsored by DOE's Office of Biological and Environmental Research and located at Pacific Northwest National Laboratory, which is operated for DOE by Battelle under Contract DE-AC06-76RLO 1830. L. S. W. is an Alfred P. Sloan Foundation Research Fellow.

[1] D. M. Cox, D. J. Trevor, R. L. Whitten, E. A. Rohlfing, and A. Kaldor, J. Chem. Phys. **84**, 4651 (1986).
[2] A. I. Boldyrev and P. v. R. Schleyer, J. Am. Chem. Soc. **113**, 9045 (1991).
[3] V. G. Zakrzewski, W. von Niessen, A. I. Boldyrev, and P. v. R. Schleyer, Chem. Phys. Lett. **197**, 195 (1992).
[4] H. Wu, X. Li, X. B. Wang, C. F. Ding, and L. S. Wang, J. Chem. Phys. **109**, 449 (1998).
[5] M. F. Jarrold and J. E. Bower, J. Chem. Phys. **87**, 1610 (1987).
[6] P. v. R. Schleyer and A. I. Boldyrev, J. Chem. Soc. Chem. Commun. **21**, 1536 (1991).
[7] S. K. Nayak, B. K. Rao, P. Jena, X. Li, and L. S. Wang, Phys. Rev. B (in press).
[8] A. Nakajima, T. Taguwa, K. Nakao, K. Hoshino, S. Iwata, and K. Kaya, J. Chem. Phys. **102**, 660 (1995).
[9] J. Fan and L. S. Wang, J. Phys. Chem. **98**, 11814 (1994).
[10] J. Fan, J. B. Nicholas, J. M. Price, S. D. Colson, and L. S. Wang, J. Am. Chem. Soc. **117**, 5417 (1995).
[11] H. Wu, S. R. Desai, and L. S. Wang, J. Chem. Phys. **103**, 4363 (1995).
[12] H. Wu, S. R. Desai, and L. S. Wang, Phys. Rev. Lett. **76**, 212 (1996).
[13] L. S. Wang, H. Wu, S. R. Desai, and L. Lou, Phys. Rev. B **53**, 8028 (1996).
[14] H. Wu, S. R. Desai, and L. S. Wang, J. Am. Chem. Soc. **118**, 5296 (1996).
[15] L. S. Wang, H. Wu, and H. Cheng, Phys. Rev. B **55**, 12884 (1997).
[16] L. S. Wang, J. B. Nicholas, M. Dupuis, H. Wu, and S. D. Colson, Phys. Rev. Lett. **78**, 4450 (1997).
[17] S. Li, H. Wu, and L. S. Wang, J. Am. Chem. Soc. **119**, 7417 (1997).
[18] L. S. Wang, X. B. Wang, H. Wu, and H. Cheng, J. Am. Chem. Soc. **120**, 6556 (1998).
[19] H. Wu, X. Li, X. B. Wang, C. F. Ding, and L. S. Wang, J. Chem. Phys. **109**, 449 (1998).
[20] X. Li, H. Wu, X. B. Wang, and L. S. Wang, Phys. Rev. Lett. **81**, 1909 (1998).
[21] X. Li and L. S. Wang, J. Chem. Phys. **109**, 5264 (1998).
[22] L. S. Wang, H. S. Cheng, and J. Fan, J. Chem. Phys. **102**, 9480 (1998).
[23] L. S. Wang and H. Wu, in *Advances in Metal and Semiconductor Clusters. IV. Cluster Materials*, edited by M. A. Duncan (JAI, Greenwich, 1998), pp. 299–343.
[24] A. D. McLean and G. S. Chandler, J. Chem. Phys. **72**, 5639 (1980).
[25] T. Clark, J. Chandrasekhar, G. W. Spitznagel, and P. v. R. Schleyer, J. Comput. Chem. **4**, 294 (1983).
[26] M. J. Frisch, J. A. Pople, and J. S. Binkley, J. Chem. Phys. **80**, 3265 (1984).
[27] R. G. Parr and W. Yang, *Density-Functional Theory of Atoms and Molecules* (Oxford Univ., Oxford, 1989).
[28] A. D. Becke, J. Chem. Phys. **96**, 2155 (1992).
[29] J. P. Perdew, J. A. Chevary, S. H. Vosko, K. A. Jackson, M. R. Pederson, D. J. Singh, and C. Fiolhais, Phys. Rev. B **46**, 6671 (1992).
[30] R. Krishnan, J. S. Binkley, R. Seeger, and J. A. Pople, J. Chem. Phys. **72**, 650 (1980).
[31] J. Cizek, Adv. Chem. Phys. **14**, 35 (1969).

[32] G. D. Purvis III and R. J. Bartlett, J. Chem. Phys. **76**, 1910 (1982).
[33] G. E. Scuseria, C. L. Janssen, and H. F. Schaefer III, J. Chem. Phys. **89**, 7382 (1988).
[34] L. S. Cederbaum, J. Phys. B **8**, 290 (1975).
[35] W. von Niessen, J. Shirmer, and L. S. Cederbaum, Comput. Phys. Rep. **1**, 57 (1984).
[36] V. G. Zakrzewski and W. von Niessen, J. Comput. Chem. **14**, 13 (1993).
[37] V. G. Zakrzewski and J. V. Ortiz, Int. J. Quantum Chem. **53**, 583 (1995).
[38] J. V. Ortiz, V. G. Zakrzewski, and O. Dolgunitcheva, in *Conceptual Trends in Quantum Chemistry*, edited by E. S. Kryachko (Kluver, Dordrecht, 1997), Vol. 3, p. 463.
[39] GAUSSIAN 94, Revision A.1, M. J. Frisch, G. M. Trucks, H. B. Schlegel, P. M. W. Gill, B. G. Johnson, M. A. Robb, J. R. Cheeseman, T. A. Keith, G. A. Petersson, J. A. Montgomery, K. Raghavachari, M. A. Al-Laham, V. G. Zakrzewski, J. V. Ortiz, J. B. Foresman, J. Cioslowski, B. B. Stefanov, A. Nanayakkara, M. Challacombe, C. Y. Peng, P. Y. Ayala, W. Chen, M. W. Wong, J. L. Andres, E. S. Replogle, R. Gomperts, R. L. Martin, D. J. Fox, J. S. Binkley, D. J. Defrees, J. Baker, J. J. P. Stewart, M. Head-Gordon, C. Gonzales, and J. A. Pople, GAUSSIAN, Inc., Pittsburgh, PA, 1995.
[40] H. A. Jahn and E. Teller, Proc. R. Soc. London, Ser. A **161**, 220 (1937).
[41] E. R. Davidson, J. Am. Chem. Soc. **99**, 397 (1977).
[42] T. C. Thompson, D. G. Truhlar, and C. A. Mead, J. Chem. Phys. **82**, 2392 (1985).
[43] MO pictures were made using MOLDEN3.4 program, G. Schaftenaar, MOLDEN3.4, CAOS/CAMM Center, The Netherlands, 1998.